INTEGRAL

Announcement of Opportunity for Observing Proposals (AO-2)

IBIS Observer's Manual

Written by: P. Barr & E. Kuulkers

Integral Science Operations, ESTEC

Based upon inputs from:
P. Ubertini, IBIS Co-P.I., IAS-CNR, Rome
F. Lebrun, IBIS Co-P.I., CEA, Saclay
A. Bazzano, IAS-CNR, Rome
L. Natalucci, IAS-CNR, Rome
J. Lockley, University of Southampton

15 July 2003

Issue 2

Ref. nr. INT-SOC-DOC-021

This page was intentionally left blank

Table of Contents

This page was intentionally left blank

I. Introduction

IBIS (**I**mager on **B**oard the **I**NTEGRAL **S**atellite) is one of the two prime instruments of the INTEGRAL scientific payload.

IBIS is a gamma-ray telescope which is able to observe celestial objects of all classes ranging from the most compact galactic systems to extra-galactic objects, with powerful diagnostic capabilities of fine imaging, source identification and spectral sensitivity in both continuum and lines. It covers the entire energy range from about 15 keV to several MeV, and it can localise weak sources at low energies to better than a few arcminutes accuracy.

Table 1 gives an overview of the scientific capabilities of IBIS. Note that the line sensitivity values are those as determined pre-launch.

Table 1:

Operating energy range	15 keV - 10 MeV
Continuum sensitivity, in photons cm^{-2} s^{-1} keV^{-1} (3σ detection, $\Delta E=E/2$, 10^5 s integration) *	2×10^{-6} @ 100 keV 1.5×10^{-6} @ 1 MeV
Line sensitivity, in photons cm^{-2} s^{-1} (3σ detection, 10^6 s integration)	1.9×10^{-5} @ 100 keV 3.8×10^{-4} @ 1MeV
Energy resolution (FWHM)	8% @ 100 keV 10% @ 1 MeV
Angular resolution (FWHM)	12'
Point source location accuracy (90% error radius)	30" @ 100 keV 1' @ 1 MeV
Absolute timing accuracy (3σ)	62 μs - 30 min
Field of view	9^o x 9^o (fully coded) 29^o x 29^o (zero response)

* Note that the continuum sensitivities given are statistical limits only, based on the in-flight measured background.

Imaging is performed using coded mask technology. There are two detectors operating simultaneously; the **I**ntegral **S**oft **G**amma-**R**ay **I**mager, ISGRI, a semi-conductor array optimised at lower energies, and the **PI**xellated Ceasium Iodide (**CsI**) **T**elescope, PICsIT, a crystal scintillator, for higher energies. The energy ranges covered by ISGRI and PICsIT overlap considerably; ISGRI covers the range 15 keV - 1 MeV; PICsIT covers 175 keV - 10 MeV. ISGRI is more efficient below about 200 keV (factor ~3); PICsIT is more efficient at higher energies (e.g. a factor ~3 at 511 keV), but the different background levels in the two detectors must also be factored into sensitivity calculations (as discussed in section VI.2).

Sections II.1, V.3 and Chapter VI of this document give the prospective observer a top-level description about the overall design and scientific capabilities of IBIS, to assist in the writing of observing proposals; we recommend these to be studied first.

The rest of Chapter II contains a more detailed engineering description of the instrument. Chapter III gives information about how IBIS actually works, while Chapter IV describes the scientific mode of the instrument. Finally, parts 1 and 2 of Chapter V describe the in-orbit behaviour of IBIS and how it is calibrated.

II. Description of the instrument

1. Overall design

IBIS is a gamma-ray imager operating in the energy range 15 keV to 10 MeV, with two simultaneously operating detectors covering the full energy range, located behind a Tungsten mask which provides the encoding.

The coded mask is optimised for high angular resolution. As diffraction is negligible at gamma-ray wavelengths, the angular resolution of a coded-mask telescope is limited by the spatial resolution of the detector array. The angular resolution of a coded mask telescope is defined by the ratio between the mask element size and the mask-to-detection plane distance (in this case 3.2 m). The IBIS detectors are made of a large number of small, fully independent pixels.

The detector features two layers, ISGRI and PICsIT: the first is made of Cadmium-Telluride (CdTe) solid-state detectors and the second of Caesium-Iodide (CsI) scintillator crystals. This configuration ensures a good broad line and continuum sensitivity over the wide spectral range covered by IBIS. The double-layer discrete-element design of IBIS allows the paths of interacting photons to be tracked in 3D if the event involves detection units of both ISGRI and PICsIT. The application of Compton reconstruction algorithms to these types of events (between a few hundred keV and a few MeV) allows an increase in signal to noise ratio attainable by rejecting those events unlikely to correspond to source photons outside the field of view.

The detector aperture is restricted, in the hard X-ray part of the spectrum, by passive shielding covering the distance between mask and detector plane. An active BGO scintillator VETO system shields the detector bottom as well as the four sides up to the bottom of ISGRI.

Figure 1 shows a cut-away drawing of the various components of IBIS (except the mask and tube).

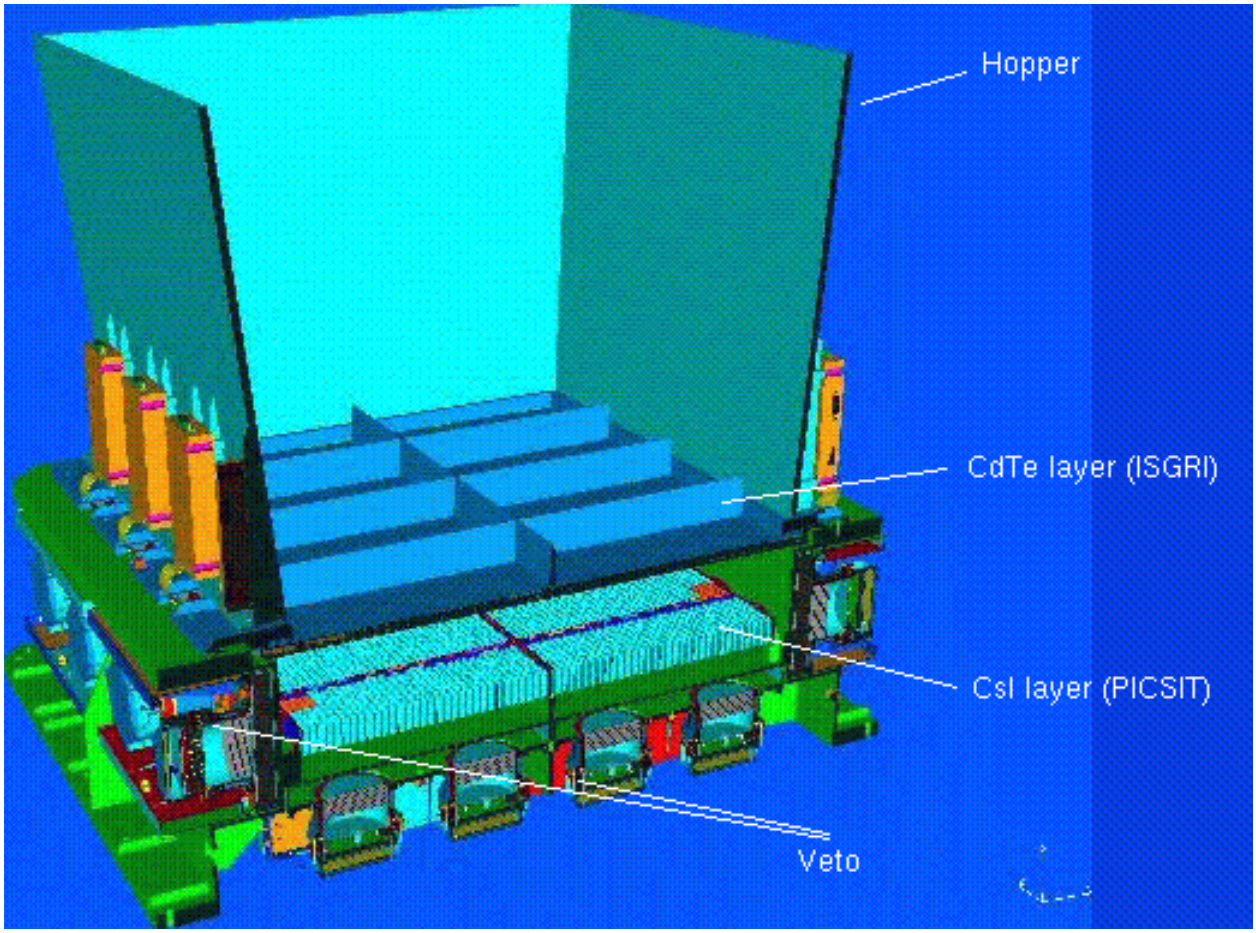

Figure 1. Cutaway drawing of the IBIS detector assembly, together with the lower part of the collimator ("Hopper"). The coded mask (not shown) is located 3.2 m above the ISGRI detector plane.

2. Imaging System

2.1 The Collimator

In order to maintain the low-energy response of IBIS despite the dithering needed for SPI (see the *Integral Manual*), the collimation baseline consists of a passive lateral shield that limits the solid angle (and therefore the cosmic gamma-ray background) viewed directly by IBIS detector in the full field of view up to a few hundreds of a keV.

The tube collimation system is implemented with three different devices:

The Hopper: Four inclined walls starting from the detector unit with a direct interface to the IBIS detector mechanical structure. The inclination of the hopper walls should ideally join the mask size, but the true inclination takes into account the presence of the Calibration System and the mechanical constraints. The hopper walls reach 550 mm out from the ISGRI top plane (850 mm from the PLM base), while the actual height is 530 mm. The shielding effect is obtained with Tungsten foils embedded in the four hopper walls. The hopper walls thickness is 1 mm. The hopper is not physically connected to the payload module structure.

The Tube: The Tube is formed by four payload module walls shielded with glued Lead foils. Two of the tube walls (-/+Z axis) are inclined (by 3.472 degrees to the vertical) in order to follow as closely as possible the inclined ideal tube shape, whilst the Y-axis walls are vertical, as shown in Figure 1. In particular the actual inclination of the Z walls is defined by the interface requirements with the hopper: the Z Tube walls stop at 20 mm in the horizontal plane from each upper edge of the hopper walls (i.e. at 850 mm from the Payload Module, PLM, base).

The additional side shielding on the mask: Four strips of 1 mm thick Tungsten provide shielding from the diffuse background in the gaps between the mask edges and the top of the tube walls.

2.2 The Mask

The IBIS Mask Assembly is rectangular with external dimensions of 1180 x 1142 x 114 mm^3, and consists of three main subsystems: the Coded Pattern, the Support Panel and the Peripheral Frame with the necessary interface provisions.

The Coded Pattern is square, of size 1064 x 1064 x 16 mm^3, made up of 95 x 95 individual square cells of size 11.2 x 11.2 mm^2.

The cells form a modified uniformly redundant array (MURA) coded pattern of 53 x 53 elements. Approximately half of the cells are opaque to photons in the operational energy range of the IBIS instrument, offering a 70% opacity at 1.5 MeV. The other half of the cells are open, i.e. with an off-axis transparency of 60% at 20 keV. Figure 2 shows the mask pattern.

The Support Panel includes those additional elements to support the code pixels, providing the necessary stiffness and strength to overcome the launch environment and the in-orbit operational temperatures. *The Peripheral Frame* reinforces the sandwich panel.

The mechanical interfaces with the INTEGRAL PLM also provide extra Tungsten shielding to the diffuse background through the gaps between the mask edges and the payload vertical walls.

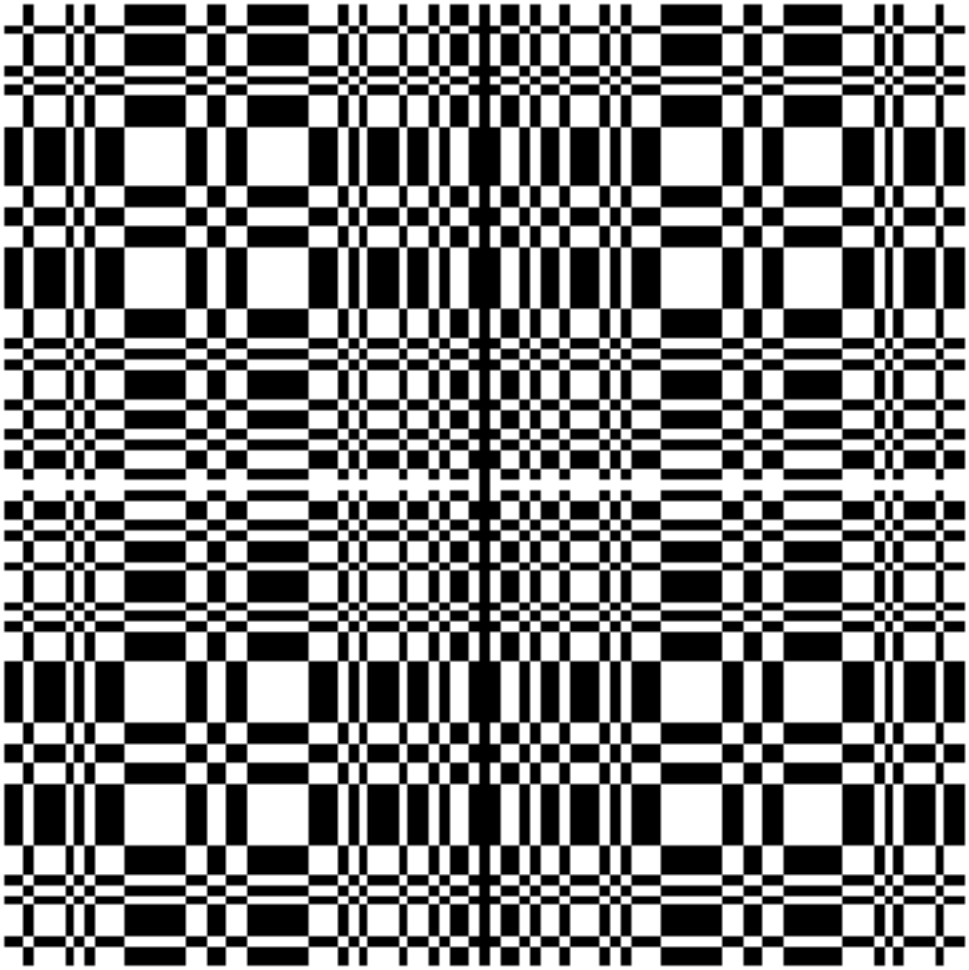

Figure 2. The IBIS coded mask pattern.

3. Detector assembly

The ISGRI and PICsIT detectors are layered with respect to each other, with PICsIT 'under' ISGRI with respect to the coded mask (and hence the astronomical source).

3.1 Upper detector layer: ISGRI

Cadmium Telluride (CdTe) is a II-VI semi-conductor operating at an ambient temperature; 0^o +/- 20^o C is the optimum range. With their small area, the CdTe detectors are ideally suited to

build a pixellated imager with good spatial resolution. On the other hand, their small thickness (necessary to achieve good energy resolution) restricts their use to the low energy domain (50% efficiency at 150 keV). Providing spectral performances intermediate between that attained by the cooled germanium spectrometers and those of the scintillators, the CdTe can be used well in the low energy domain (down to ~15 keV).

The CdTe layer is made of 8 identical Modular Detection Units (MDUs) each having 2048 pixels which are read out by 512 Application Specific Integrated Circuits (ASICs) (4 channels per ASIC). Each MDU is connected independently to a Detector Bias Box (DBB) and to a Module Control Electronics (MCE) system which ensures the A/D conversion and provides other on-board processing such as event filtering and active pixel monitoring.

The specifications are:

- Pixel (CdTe crystal) dimension: 4 x 4 mm^2, 2 mm thick
- Spacing between pixels: 600 μm (4.6 mm centre-to-centre)
- Minimum assembly: polycell of 16 pixels (4 x 4)
- MDU: 128 polycells (16 x 8)
- Layer: 8 MDUs (128 x 128 detection units)
- Total sensitive area: 2621 cm^2 (128 x 128 x 16 mm^2).

The CdTe layer is located at 294 mm above the PLM base plane and its overall thickness is about 15mm.

3.2 Lower detector layer: PICsIT

Caesium Iodide (CsI) is a I-VII scintillation crystal. The main characteristics of the layer are:

- Pixel (CsI(Tl)) crystal dimension: 8.55 x 8.55 mm^2, 30 mm thick
- Spacing between pixels: 550 μm (9.2 mm centre-to-centre)
- Minimum assembly (ASIC): 16 detection units
- Module: 512 detection units (32 x 16)
- Layer: 8 Modules (8 x 512)
-Total sensitive area: 2994 cm^2 (pixel area x 4096).

The CsI(Tl) bars are optically bonded to custom-made low-leakage silicon PIN photodiodes. The design provides a high degree of modularity. The CsI(Tl) layer is divided in 8 rectangular modules of 512 detector elements, each module being integrated into a stand-alone testable sub-system. The CsI modules have the same cross-sectional shape as those of the CdTe.

4. Veto shield

The Veto shield is crucial to the operation of IBIS. IBIS uses anti-concidence logic to accept or reject detected events as real photons in the field of view, or background particles or photons propagating through, or induced in, the spacecraft.

The sides, up to the ISGRI bottom level, and rear of the stack of detector planes are surrounded by an active Bismuth Germanate (BGO) veto shield. Like the detector array, the Veto shield is modular in construction.

There are 8 lateral shields, i.e. 2 modules per side, and 8 bottom modules.

Each Veto Detector Module (VDM) includes:

- the BGO crystal and related housing
- two photomultiplier tubes (PMTs) optically coupled to the BGO and assembled with the dedicated Front End Amplifiers and high voltage (HV) divider
- one HV Power Supply
- one Veto Module Electronics box for Module control
- internal harness.

The high density and mean Z of the BGO ensures that a thickness of 20 mm is sufficient to reduce the detector background, due to leakage through the shielding of cosmic diffuse gamma–ray background and gamma–rays produced in the spacecraft, to less than the sum of all other background components.

5. Electronics

5.1 Analog Front End Electronics (AFEE)

Charge collection, signal filtering, and amplification are all performed by the Application Specific Integrated Circuits (ASICs) on both ISGRI and PICsIT. In ISGRI, the 16384 individual detectors (pixels) are grouped into 'polycells'. A polycell is a hybrid circuit which receives a signal from 16 detectors via 4 ASICs, and is the basic assembly unit of a detector module.

5.2 Module Control Electronics (MCE) and PICsIT Electronic Box (PEB)

The MCE and PEB perform receipt, checking and execution of telecommands for ISGRI and PICsIT, respectively. They also collect and format the housekeeping data and process the analogue and digital data (energy and rise time). An important function of the MCE is to monitor the CdTe noise levels. In-flight a CdTe detector can become noisy and trigger the relevant MCE too

frequently, causing a large dead time with unacceptable loss of photons. Therefore the MCE monitors, in real time, the relative counting rates of each CdTe polycell. If a polycell exhibits noise, the MCE will, if necessary, switch it off. It can be subsequently reactivated and checked from the ground.

5.3 On-Board Calibration Unit

IBIS contains an on-board collimated radioactive ^{22}Na source. This allows regular calibration of PICsIT at both the 511 keV line and 1275 keV (calibration to better than about 1% in 1-2 orbits). ISGRI can also use the 511 keV line, albeit at lower efficiency.

5.4 Digital Front End Electronics (DFEE) and 'FIFO'

The DFEE sits behind the AFEE and processes the ASICs output for the 'first-in, first-out' (FIFO) data manager. FIFO sorts the events from different modules according to their true arrival time in the detector plane for transmission to the DPE/HEPI (see below). The DFEE also monitors the FIFO and instructs it when to send data to the DPE.

5.5 Data Processing Electronics (DPE) and Hardware Event Processor (HEPI)

The detector electronics chain ends at the DPE and the HEPI. The HEPI performs the data histogramming and generates the data structures for the DPE. The DPE handles all the interfaces between the instruments and the spacecraft for both uplink and downlink, for example, packetting the data for the On-Board Data-Handling System for transmission to ground.

III. How the instrument works

Photons are detected by three methods:

(i) Direct detection in ISGRI.

A photon is stopped in a single pixel of the semi-conductor, generating an electric pulse.

(ii) Direct detection in PICsIT.

A photon passes through ISGRI and is stopped in PICsIT, generating one or more scintillation flashes. PICsIT single and multiple (see below) are distinguished accordingly.

(iii) Multiple events.

Photons arriving in either ISGRI or PICsIT produce secondary photons via Compton scattering, subsequently detected in either detector layer. Multiple events in ISGRI are rejected. In Figure 3 we show the efficiencies of the various detection techniques.

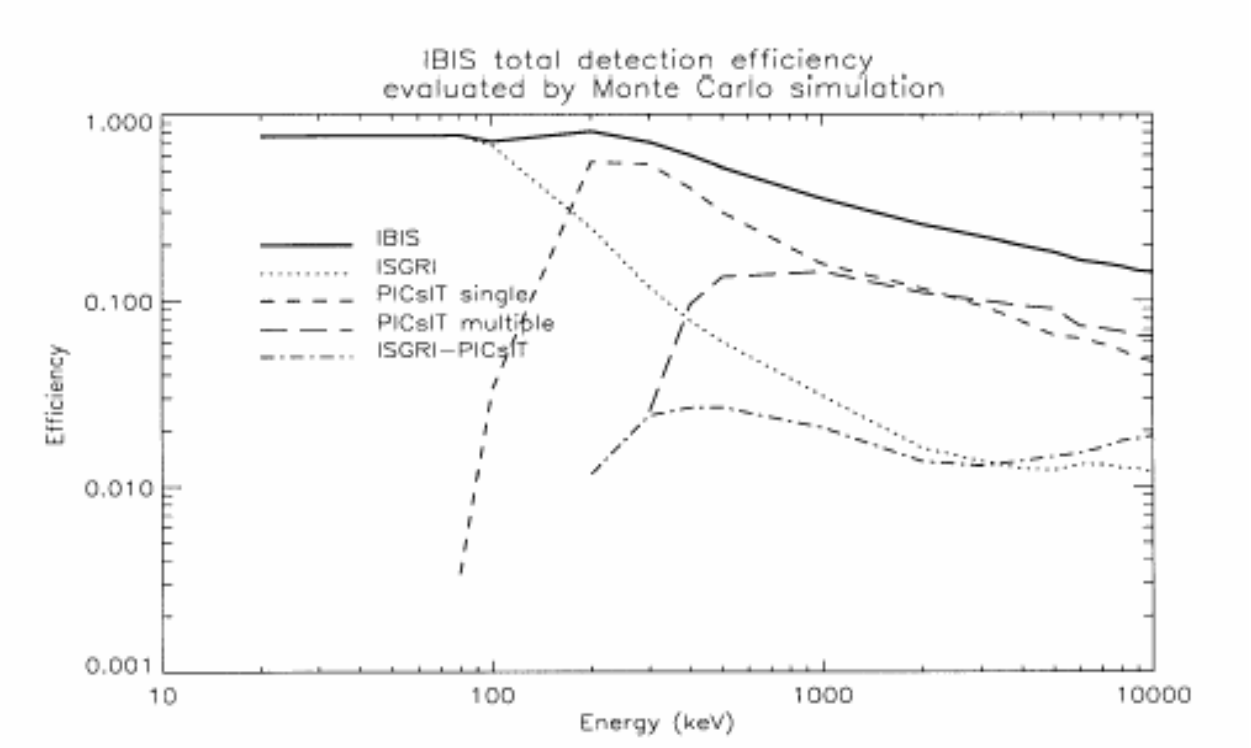

Figure 3. IBIS efficiencies for the various detection techniques, as evaluated pre-launch. "ISGRI-PICsIT" refers to the Compton events.

1. Imaging

Both ISGRI and PICsIT record the (x,y) coordinates of each event registered in the corresponding layer, to build up an image. The anti-concidence VETO is used to reject background events.

The coded mask produces a shadowgram. Photons from the source and the background are distributed across the entire field of view, but cross-correlation techniques allow the full image to be reconstructed for the fully coded field of view (FCFOV: 9^o x 9^o) at each pointing. For the partially coded field of view (PCFOV: out to 29^o x 29^o) special cleaning techniques must be applied to the data to properly reconstruct the image.

The actual sky coverage in an observation depends on the dither pattern. For example, during a 5 x 5 dither pattern a 37^o x 37^o field is imaged out to zero response, while a 17^o x 17^o region is sampled (at least partly) with full coding.

2. Spectroscopy

2.1 Direct detection in ISGRI

In principle, the amplitude of the pulse yields the energy of the incident photon. However, above 50 keV the energy determined is not just a function of the pulse height but also the pulse rise time, so both are used to determine the energy of the incident photon. In addition, the resulting line profile (energy resolution) is no longer Gaussian, but more similar to a Lorentzian. The energy resolution depends on the operating temperature, and also on the bias voltage; the bias voltage has to be optimised as a trade-off between high resolution but more noise (high voltage) or lower noise but lower resolution (low voltage).

2.2 Direct detection in PICsIT

The energy of the incident photon is derived, in each crystal bar, from the intensity of the flash recorded in the photodiode. The energy resolution of PICsIT is a function of the signal-to-noise of the events, the electronic noise at low energies, and the light output.

2.3 Multiple events

For true Compton events (i.e. real gamma-ray photons) the energy is determined from the sum of energies recorded for the initial event and in the detection of the scattered photon.

The Compton event rate has been modeled but the predictions are uncertain. *We recommend that when using the observing time estimator, only the direct ISGRI and PICsIT calculations are used for the basis of an observing proposal.* Any increase in sensitivity available from Compton events should be regarded as a bonus.

3. Timing

The ISGRI time resolution is 62 μs for each detected event. PICsIT spectra and images are accumulated every 1800-3600 seconds depending on the (flexible) dithering time; a spectrum alone (but with low resolution - from two to eight energy channels) is available every several milliseconds. See also Chapter IV.

4. Polarimetry

In principle, the multiple events in adjacent PICsIT cells can be used to determine the polarisation of the incident photons, because of the Klein-Nishina cross-section with polariation angle. However, at present polarisation is not feasible, and it is, therefore, not offered in this AO.

IV. Overview of observing modes and parameters

IBIS has several observing modes, for engineering and calibration purposes. However, for scientific use there is only one operating mode, i.e. Science Mode. The Science Mode has no user-selectable parameters.

In Science Mode, ISGRI registers and transmits events on a photon-by-photon basis, i.e. every event is tagged with its (x,y) position on the detector plane, event energy (from the pulse height and rise time) and event time.

PICsIT, in principle, can also operate in photon-by-photon mode. However, given the higher background compared to ISGRI, with the available telemetry there would be unacceptable data losses. Therefore, the standard mode for PICsIT is 'histogram'. Images and spectra (full spatial resolution, 256 energy channels) are accumulated for 1800-3600 seconds (depending on the flexible dithering time) before transmission to ground. There is no time-tagging internal to the histogram, i.e. spectral imaging has a time resolution of 1800-3600 seconds only.

Additionally, coarse spectra without imaging information are accumulated by PICsIT and transmitted with far higher time resolution. However, without imaging information their usefulness is limited to observations of very strong sources where the source count rate dominates the background. The time resolution and the number of energy channels for this spectral timing data can be commanded from the ground. The time resolution can take values between 500 ms to 0.976 ms; the current default is 1.95 ms and 4 energy channels.

V. Performance of the instrument

1. Components and sources of instrumental background

For most astronomical sources, the background will be higher than the measured source intensity.

The principal sources of background in IBIS are:

- for ISGRI at lower energies (down to about 100 keV), the diffuse cosmic gamma-ray background;

- for ISGRI at higher energies, and for PICsIT, the energetic particle background induced by cosmic ray hadrons interacting with the solid body of INTEGRAL - radioactive decay.

Other effects which influence the background are e.g. solar activity and VETO performance. The particle background varies over the solar cycle. It is lowest at solar maximum, when the higher solar magnetic field inhibits the propagation of cosmic rays into the inner solar system. It is a factor of ~2 higher at solar minimum.

The (background) detector images are strongly structured (apart from bad or dead pixels). They are currently being evaluated in order to be taken into account in the background subtraction algorithms.

Already since the first instrument activation frequent bursts of counts in the PICsIT count rate have been observed. In the accumulated detector images they are seen as tracks of bright pixels; they indicate that these events are related to the interaction of cosmic rays with the detector. The contribution of these cosmic rays induced triggers to the total PICsIT background is of the order of 10%. However, these triggers are mainly effective at low energy channels (up to about 30% of the total background).

The observed background rates compared to the Crab on-axis count rates are given in Table 2. The background rates quoted here are determined in-flight using calibration observations.

Table 2: Background rates compared to the Crab rates

Instrument	Background (Solar Max) cts s^{-1}	Crab on-axis cts s^{-1}
ISGRI	600	220
Compton	135	n/a
PICsIT	3650	6.7

IBIS is located next to the SPI and JEM-X instruments that have similar configurations. Since gamma-rays are highly penetrating, it is possible for them to pass through parts of the spacecraft or instrument structures, as well as coded masks and to be detected by the gamma-ray instruments. Therefore, off-axis gamma-rays (effectively those with energies above ~300 keV) that pass through the SPI coded mask may cast a shadow of this mask onto the IBIS detectors. This combination is often referred to as the ''SPIBIS'' instrument. Although it effectively increases the field of view of IBIS, a bright gamma-ray source would thus add additional counts and modulation to the IBIS histogram, which considerably complicates the image reconstruction.

The SPIBIS effect has been calibrated before launch. Currently, the ISOC avoids scheduling sources when either of the three brightest sources/regions, i.e. Crab, Cyg X-1 or the Galactic Center region, are visible by IBIS through the SPI mask. This ensures that the observation is uncontaminated by a possible SPIBIS effect.

2. Instrumental characterisation and calibration

The ISGRI and PICsIT detectors were calibrated in-orbit during the INTEGRAL commissioning phase. At present the calibration is good up to the 10% level up to ~300 keV. During routine operations observations of the Crab nebula and/or Cyg X-1 are, and will be, performed, to enable regular verification of the detector uniformity and its energy response, as well as enhancing the calibration.

At high energies (typically > 1 MeV), the background so strongly dominates the flux of any calibration source that a large amount of data is needed. It was not possible to take sufficient measurements in the few weeks available for commissioning phase. Therefore, data accumulated through the routine operations phase are used to extend the calibration to ~10 MeV.

The instrument characteristics will also be checked after strong disturbing events such as solar flares. The energy response and spectral resolution is monitored on long time-scales using the de-excitation lines at 511 keV and 1275 keV emitted by the on-Board ^{22}Na calibration source, and at 59.3 keV using the background-induced Tungsten fluorescence line from the coded mask and hopper walls.

3. Measured performance

3.1 Imaging resolution

In the FCFOV the off-axis response (sensitivity, spatial resolution) is fairly uniform, at least above ~30 keV (at the lowest energies the off-axis transparency of the mask falls off quickly). However if a 5 x 5 dither pattern is used there is a slight (~2%) loss in overall sensitivity averaged over the dither pattern.

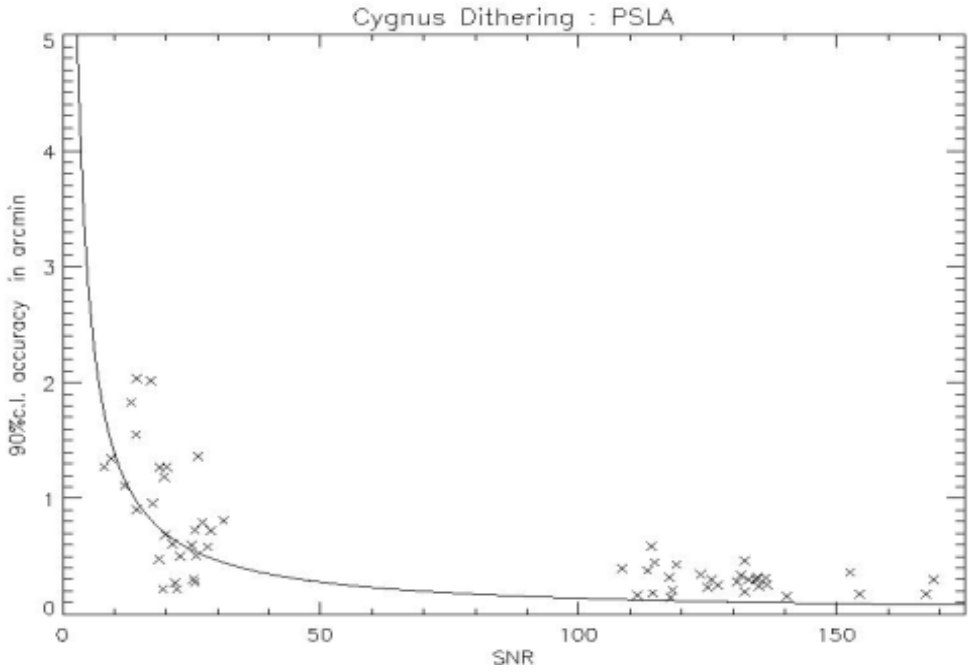

Figure 4. The point-source location accuracy (PSLA; 90% confidence level accuracy) for ISGRI using in-flight calibration observations of Cyg X-1 and Cyg X-3. The expected curve (continuous line) is also shown.

The angular resolution of IBIS is 12' FWHM. However a feature of the mask is that the centroiding accuracy for a point source can be far finer. Figure 4 shows the measured point source location accuracy (PSLA) in ISGRI as a function of signal-to-noise ratio from observations (points) and theory (line). The absolute localisation (after misalignment correction) is better than 1-1.5' for bright sources. The PICsIT PSLA is a factor ~2 coarser than that of ISGRI.

3.2 Spectral resolution

The spectral resolution of IBIS has been measured during tests on the engineering model, as well as in-flight. Figure 5 shows the ISGRI spectral performance, both measured pre-launch and theoretical. The measurements deviate from the model at higher energies because no rise-time correction was applied. The evaluation of the ISGRI in-flight spectral performance is still in progress.

Figure 6 shows the PICsIT spectral resolution, as determined in-flight. The expected, theoretical, values are determined from measurements which were taken from the engineering model tests. The in-flight data do not show any degradation or changes in the PICsIT spectral performance so far.

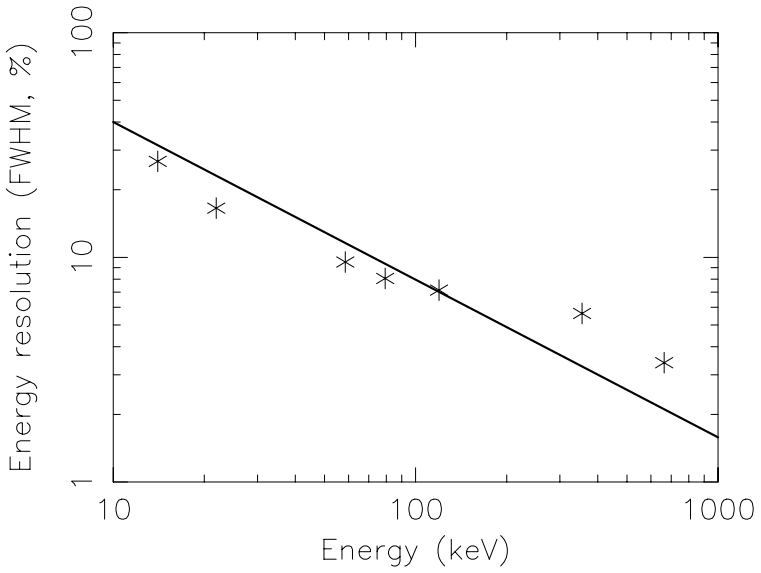

Figure 5. The energy resolution of ISGRI as determined before launch. Solid line; theoretically expected values; points (stars): values measured on the engineering model. There is no evidence that the energy resolution has degarded or changed in-flight. Note that above about 200 keV, PICsIT is more sensitive than ISGRI, and the PICsIT energy resolution shown in Figure 6 is more relevant.

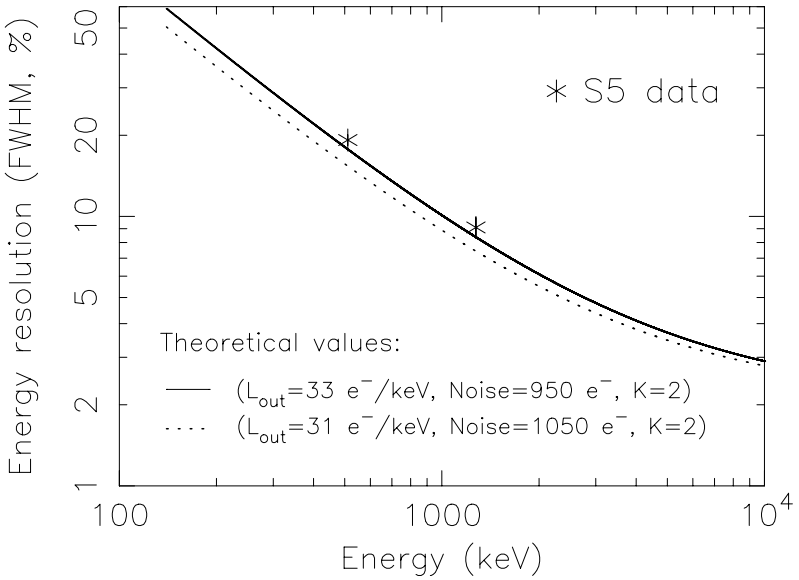

Figure 6. PICsIT energy resolution as measured in-flight using Calibration Unit (S5) data. Also shown are the theoretical expectations as determined from pre-flight tests using an engineering model (EM). The electronic noise values ("Noise") refer to one ASIC only; a 10% increase is expected when extrapolating to the complete detector electronic chain.

3.3 Sensitivity

The full calculations for continuum and line sensitivities are in principle given by the following equations:

V-3.3.1 Continuum:

$$S_c = n_\sigma [TA\Delta E\, \varepsilon_T \varepsilon_I (\vartheta_o-\vartheta_c)^2]^{-1}\{n_\sigma(\vartheta_o+\vartheta_c)^2 + [n_\sigma{}^2(\vartheta_o-\vartheta_c)^2 + 4(\vartheta_o-\vartheta_c)^2\, T\Delta E\, AB]^{0.5}\}$$

V-3.3.2 (Narrow) line:

$$S_l = n_\sigma [TA\varepsilon_p \varepsilon_I (\vartheta_o-\vartheta_c)^2]^{-1}\text{-}\{n_\sigma(\vartheta_o+\vartheta_c)^2 + [n_\sigma{}^2(\vartheta_o-\vartheta_c)^2 + 4(\vartheta_o-\vartheta_c)^2\, T\delta E\, AB]^{0.5}\},$$

where

S_c is the continuum sensitivity in photons cm^{-2} sec^{-1} keV^{-1},
S_l is the line sensitivity in photons cm^{-2} sec^{-1},
n_σ is the number of sigma,
ΔE is the energy bin (for continuum),
δE is the energy resolution,
A is the detector area,
ε_p, ε_T are the peak and total efficiencies,
ε_I is the imaging efficiency, a function of the coding noise and dither pattern,
B is the background countrate in counts cm^{-2} sec^{-1} keV^{-1},
ϑ_o, ϑ_c are the open and closed mask element transparencies, and
T is the observation duration.

Note that for a broad line with a FWHM of ΔE keV, the sensitivity is reduced by $(\Delta E/\delta E)^{1/2}$.

In Chapter VI we show the sensitivity curves in Figures 8 and 9, thus calculated, for ISGRI and PICsIT separately, and how they may be used to estimate signal-to-noise ratios and observing times. However, we stronly recommend the final proposed times always to be calculated using the on-line observing time estimator (OTE); those are the only values which will be used in the technical feasibility check of the proposal performed for the Time Allocation Committee (TAC) by the ISOC.

PLEASE NOTE: the continuum sensitivities given in Chapter VI are for ***monochromatic flux density (photons cm^{-2} s^{-1} keV^{-1})***, while the input for the observing time estimator (OTE) is in ***broad-band flux (photons cm^{-2} s^{-1})*** within a user-defined energy range.

3.4 Timing capabilities

The *time resolution* in ISGRI is 62 μs. For PICsIT, imaging and spectral histograms are collected every 1800-3600 seconds (depending on the flexible dithering time) - there is no finer time resolution available inside the histogram. The spectral timing data of PICsIT (no imaging!) will be accumulated every few ms; the resolution can be selected from ground and can take a value between 0.976 and 500 ms. The value used in routine operations is currently 62 μs. Once selected, it will apply to all PICsIT observations.

The *absolute timing accuracy,* i.e. the barycentric correction to event times measured in IBIS, depends on not just the time resolution, but also on time frame synchronisation in the instrument and spacecraft subsystems, and the uncertainty in the spacecraft position around the orbit. Current calculations indicate a 1σ uncertainty of 61 μs and 3σ uncertainty of 92 μs. This will be evaluated in-flight via dedicated pulsar observations.

VI. Observation "Cook book"

1. Astronomical considerations on the use of the instrument

In this section we present some typical examples of the kinds of scientific studies suitable for IBIS. The selection is by no means exhaustive.

Black Holes

IBIS can detect all currently known persistent black-hole (BH) candidates in our galaxy.

IBIS will be used to investigate whether BH binary systems are characterised by distinctive X/gamma−ray signatures. For example, are their spectra significantly harder than those from neutron star systems - is the bulk of their luminosity indeed in the soft gamma−ray band? Can the spectral turnover be measured and the total luminosity constrained?

QPOs have also been measured in BH systems - e.g. Cyg X-1 - and could provide further important diagnostic of the structure of the inner edge of the accretion disk, and possibly also the BH mass itself.

IBIS will also be able to detect any Galactic hard X/gamma−ray transient in outburst within the few minutes exposures provided by the routine Galactic Plane Survey (GPS) or the Galactic Centre Deep Exposure (GCDE). Subsequent follow-up longer observations can monitor the light curve of the transient, its spectral evolution, and possible transient lines with unprecedented spectroscopic quality.

Of particular interest in such transients is the appearance of broad transient lines. For example, Nova Muscae 1991 (GS 1124-68) showed a broad line at 480 keV - redshifted annihilation? - and another spectral feature near 200 keV, possibly due to Compton backscattering. IBIS will measure such features with good statistical accuracy on timescales of minutes rather than hours, allowing the study of the rapidly changing geometry and physical conditions in the immediate vicinity of black hole systems.

Neutron Stars

Neutron stars (NS) - both in binary systems and isolated NS (e.g. pulsars) - will be objects of prime interest for IBIS.

For example, observations of the Galactic Centre region with SIGMA, BeppoSAX and RXTE indicate that X-ray bursters are a newly identified class of soft gamma-ray sources.

In addition, the good spectral resolution and large collecting area at low energy will enable the study of cyclotron lines from magnetized NS in great detail, e.g phase-resolved line shapes/ widths.

The good sensitivity at higher energy will allow detection of isolated pulsars in the MeV region, where their properties are so far poorly measured.

It is worth noting in general that the soft gamma-ray domain is probably the best region to ee" the accretion at work close to the compact object.

Supernovae

In most cases, the line sensitivity of IBIS is independent of the intrinsic line width and IBIS ovides a powerful imaging complement to SPI - studying the spatial distribution of hot spot line nission from supernova remnants and in the galactic plane in general, while SPI provides fine ectroscopy. Also, hidden young SNR will show up as emission-line point sources.

Extragalactic studies

A main result of CGRO and BeppoSAX observations of AGN is that their broad-band con- ıua strongly depends on their AGN type. Figure 7 provides an estimate of the number of AGN tectable by IBIS assuming two standard observation times; 10^5 s for detection up to 100 keV, ıd 10^6 s for detection up to the MeV region.

At *low energies* these will be mostly Seyferts. Although it is known that their spectra fall off ımewhere above ~50 keV (but below ~1 MeV), the details of this cut-off are still highly uncertain, mainly due to difficulties in fitting complex models over a limited (due to the lack of sensitive high-energy observations) energy band. Based on the existing 2-10 keV log N/log S distribution IBIS should be able to detect about 200 Seyferts across the whole sky in a typical 1 day exposure to 100 keV, and about 20 objects out to 1 MeV (depending on where the turnover is) thus allowing spectral studies to be performed on a quite large sample of sources. In comparison, the first X-ray surveys in the 1970's (Uhuru, Ariel V) found ~50 AGN over the whole sky. Another intriguing issue which IBIS will address is whether there is a large population of Compton-thick AGN visible above 30 keV.

At *higher energies* most of the sources will likely be blazars, whether MeV peaked or TeV peaked. The main interest with INTEGRAL is the determination of the spectral characteristics from keV to MeV energies (spectral breaks? hard tails?). To this end observations would probably be longer (up to 10^6 s depending on the source). However, it is worth noting that longer exposures would as a by-product find a number of serendipitous sources (typically ~4 sources per field of view?)!

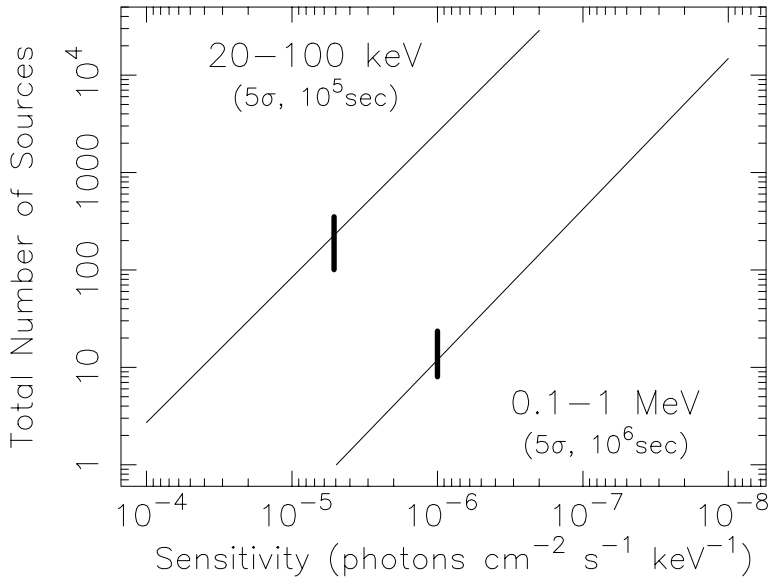

Figure 7. Number of AGN visible to IBIS in soft and hard gamma-rays, assuming the 2-10 keV log N/log S measured from all-sky surveys.

2. IBIS sensitivity

Figures 8 and 9 show, respectively, the continuum (S_c) and line sensitivities (S_l), for ISGRI and PICsIT separately, as calculated from the prescriptions in Section V.3.3. The curves are for a detection of 3σ significance with an observing time of 10^5 s and 10^6 s, for the continuum and line sensistivities, respectively. The continuum sensitivity is given for ΔE=E/2. The line sensitivity is for a narrow (unresolved) line, and are pre-launch estimates; they are currently being re-evauluated. We also give the (some of the) actual values in Tables 3, 4, and 5.

2.1 How to calculate observing times

The approximate signal-to-noise ratio for a given exposure can be calculated from the sensitivity curves. As shown in equations *V-3.3.1* and *V-3.3.2*,

the continuum sensitivity scales as

$\Delta E^{-1/2}$, $t^{-1/2}$ and n_σ,

the line sensitivity as

$t^{-1/2}$ and n_σ.

Table 3: ISGRI continuum sensitivities (10^5 s exposure, 3σ detection, ΔE=E/2)

Energy (keV)	ph cm^{-2} s^{-1} keV^{-1}		Energy (keV)	ph cm^{-2} s^{-1} keV^{-1}		Energy (keV)	ph cm^{-2} s^{-1} keV^{-1}
15	12.7×10^{-6}		60	4.34×10^{-6}		300	2.71×10^{-6}
20	11.3×10^{-6}		70	3.07×10^{-6}		350	2.76×10^{-6}
25	8.69×10^{-6}		80	2.43×10^{-6}		400	2.79×10^{-6}
30	5.64×10^{-6}		90	2.12×10^{-6}		450	2.65×10^{-6}
35	4.60×10^{-6}		100	1.93×10^{-6}		500	2.78×10^{-6}
40	3.97×10^{-6}		150	2.24×10^{-6}		600	2.39×10^{-6}
45	3.67×10^{-6}		200	2.52×10^{-6}		700	2.26×10^{-6}
50	3.53×10^{-6}		250	2.66×10^{-6}		800	2.17×10^{-6}

Table 4: PICsIT continuum sensitivities (10^5 s exposure, 3σ detection, ΔE=E/2)

Start energy (keV)	End energy (keV)	ph cm^{-2} s^{-1} keV^{-1}		Start energy (keV)	End energy (keV)	ph cm^{-2} s^{-1} keV^{-1}
170	220	7.99×10^{-6}		1200	1400	1.88×10^{-6}
220	280	6.06×10^{-6}		1400	1800	1.28×10^{-6}
280	370	3.62×10^{-6}		1800	2200	1.05×10^{-6}
370	430	3.41×10^{-6}		2200	2900	0.59×10^{-6}
430	580	1.90×10^{-6}		2900	3500	0.68×10^{-6}
580	720	1.91×10^{-6}		3500	4500	0.50×10^{-6}
720	900	1.48×10^{-6}		4500	5700	0.32×10^{-6}
900	1200	1.57×10^{-6}				

Table 5: IBIS line sensitivities (ISGRI and PICsIT, 10^6 s exposure, 3σ detection)

Energy (keV)	ISGRI line ph $cm^{-2}s^{-1}$	PICsIT line ph $cm^{-2}s^{-1}$		Energy (keV)	ISGRI line ph $cm^{-2}s^{-1}$	PICsIT line ph $cm^{-2}s^{-1}$
22.5	3.34×10^{-5}			566.1	30.0×10^{-5}	28.7×10^{-5}
28.4	2.58×10^{-5}			712.6	190×10^{-5}	44.1×10^{-5}
35.7	2.04×10^{-5}			897.2	210×10^{-5}	40.2×10^{-5}
45.0	1.79×10^{-5}			1129.5		35.8×10^{-5}
56.6	1.66×10^{-5}			1421.9		31.8×10^{-5}
71.3	$1.64x\ 10^{-5}$			1790.1		56.8×10^{-5}
89.7	2.08×10^{-5}			2253.6		47.1×10^{-5}
112.9	1.79×10^{-5}			2837.1		61.4×10^{-5}
142.2	1.60×10^{-5}	281×10^{-5}		3571.7		72.6×10^{-5}
179.0	4.89×10^{-5}	19.8×10^{-5}		4496.5		84.5×10^{-5}
225.4	4.20×10^{-5}	20.6×10^{-5}		5660.7		237×10^{-5}
283.7	12.3×10^{-5}	22.6×10^{-5}		7126.5		1200×10^{-5}
357.2	20.5×10^{-5}	25.7×10^{-5}		8971.6		9440×10^{-5}
449.6	18.7×10^{-5}	23.5×10^{-5}				

So the signal-to-noise ratio achieved for a different time, t(sec), ΔE/E and continuum or line flux N_c, N_l (photons cm^{-2} s^{-1} keV^{-1} and photons cm^{-2} s^{-1} respectively), would be:

$$\mathbf{n_\sigma = 3(N_c/S_c)(2\Delta E/E)^{1/2}\ (t/10^5)^{1/2}}$$ in the continuum and *VI-2.1*

$$\mathbf{n_\sigma = 3(N_l/S_l)\ (t/10^6)^{1/2}}$$ for a narrow (unresolved) line. *VI-2.2*

If the line is broad, with a FWHM of ΔE, then the signal-to-noise ratio is reduced by $(\Delta E/\delta E)^{1/2}$, where δE is the instrumental FWHM at that energy (see Figures 5 and 6).

Note: if the 5 x 5 dither pattern is used there is a 1.8% reduction in the achieved signal-to-noise ratio compared to the above. The hexagonal dither entails no loss.

2.2 Hints and warnings

The results arising from these calculations should be treated as approximations only and should be used only for a *preliminary* feasibility check for a potential observation. The *final* observation durations - those entered into the observing proposal - should be determined with the on-line observation time estimator (OTE), accessible via the Integral Science Operations Centre web site: **http://www.rssd.esa.int/integral**.

The OTE will be used by ISOC to assess the technical feasibility of proposed observations, and advise the Time Allocation Committee (TAC) accordingly.

The continuum sensitivities (see Figures 9 and 10) are given for $\Delta E = E/2$ and can be extrapolated reliably to small energy ranges. *However, if ΔE is much greater than E/2, the assumed spectral shape can introduce artifacts into the computation and we strongly advise against using these curves for calculations over very broad energy bands.*

3. Worked-out examples

Here we give some examples of how equations *VI-2.1* and *VI-2.2* can be used to assess the feasibility of 'real' observations.

3.1 Example 1

For a hard transient with a flux of 1 Crab at 100 keV and a hard power law (photon spectral index Γ of -1) continuum above 100 keV, determine the achievable signal-to-noise ratio at 100 keV in an energy bin corresponding to the instrument FWHM at that energy.

Extrapolating the 2-10 keV flux of the Crab to the gamma-ray band, using a photon spectral index Γ of -2, a 1 Crab source has a flux at 100 keV of

$$\mathbf{N_c = 1.1 \times 10^{-3}\ photons\ cm^{-2}\ s^{-1}\ keV^{-1}}.$$

At 100 keV only ISGRI is sensitive (it is below the energy range of PICsIT). The sensitivity curve (Figure 8 or Table 3) gives a flux value at 100 keV of

$$\mathbf{S_c = 1.9 \times 10^{-6}\ photons\ cm^{-2}\ s^{-1}\ keV^{-1}}.$$

The energy resolution of ISGRI (FWHM, see Figure 5) at 100 keV is 8%;

$$\mathbf{\Delta E/E = 0.08}.$$

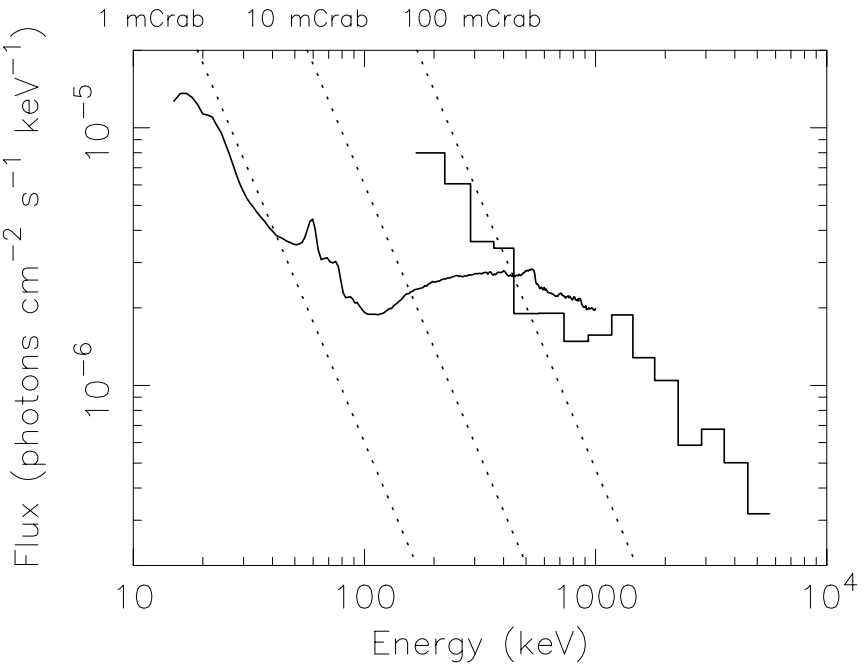

Figure 8. IBIS continuum sensitivities based on in-flight background measurements for a 10^5 s exposure, 3σ detection and continuum binned to ΔE= E/2. Systematic errors (such as background uniformity) are not taken into account. Solid line: ISGRI; solid stepped line: PICsIT (single and multiple events combined). Also shown (dotted lines) are the intensities of a 1, 10 and 100 mCrab source (photon spectral index Γ of -2).

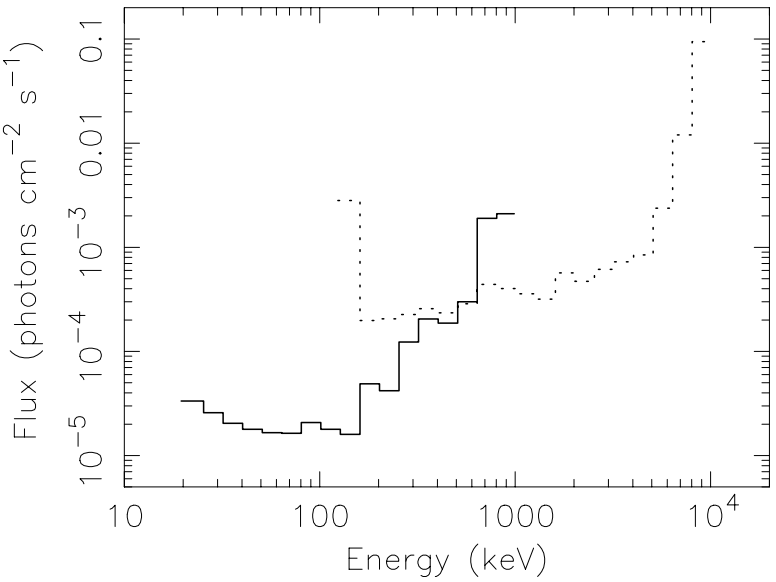

Figure 9. IBIS line sensitivities for a 10^6 s exposure, 3σ detection and an unresolved line. Solid line: ISGRI; dotted line: PICsIT. Note that the values are the same as used for AO-1; the in-flight line sensitivities are still being evaluated.

Assume an observation time of

$t = 10^4$ sec.

This results in a signal-to-noise ratio (*VI-2.1*) of

$n_\sigma = 3 \times (1.1 \times 10^{-3} / 1.9 \times 10^{-6}) \times (2 \times 0.08)^{1/2} \times (10^4 / 10^5)^{1/2} = 220\sigma$.

In comparison, the OTE indicates a 209σ detection.

3.2 Example 2

The same source as in Example 1, but at higher energies, i.e. 700 keV.

Extrapolation of the 100 keV flux with the hard power law described above gives a 700 keV flux of

$N_c = 1.6 \times 10^{-4}$ photons cm^{-2} s^{-1} keV^{-1}.

Both PICsIT and ISGRI are sensitive at 700 keV. The sensitivity curves (Figure 8 or Tables 3 and 4) indicate:

S_c (ISGRI) $= 2.3 \times 10^{-6}$ photons cm^{-2} s^{-1} keV^{-1},
S_c (PICsIT) $= 1.9 \times 10^{-6}$ photons cm^{-2} s^{-1} keV^{-1}.

The overall sensitivity compared to source flux is lower at 700 keV compared to 100 keV, so use a larger energy bin, e.g.

$\Delta E/E = 0.15$.

Again assume a 10^4s observation;

$t = 10^4$ sec.

Perform the same calculation as in Example 1;

n_σ (ISGRI) $= 36\sigma$,
n_σ (PICsIT) $= 44\sigma$.

In comparison, the OTE gives 36σ and 42σ, respectively.

ISGRI and PICsIT can be combined to increase the significance of the detection:

n_σ (total) $= (n_\sigma (\text{PICsIT})^2 + n_\sigma (\text{ISGRI})^2)^{1/2} = (36^2 + 44^2)^{1/2} = 57\sigma$.

3.3 Example 3

Observations of a recent transient to search for the ^{22}Na line at 1.275 MeV (half life of 3.5 yr).

The model-predicted line flux after outburst is

$\mathbf{N_l = 5 \times 10^{-4}\ photons\ cm^{-2}\ s^{-1}}$.

The PICsIT line sensitivity curve (Figure 9 or Table 5) indicates

$\mathbf{S_l = 3.4 \times 10^{-4}\ photons\ cm^{-2}\ s^{-1}}$.

Assume a 500 ksec observation;

$\mathbf{t = 5 \times 10^{5}\ sec}$.

Then the line is detected at (*VI-2.2*):

$\mathbf{n_\sigma = 3 \times (5 \times 10^{-4} / 3.4 \times 10^{-4}) \times (5 \times 10^{5} / 10^{6})^{1/2}} = 3\sigma$.

In comparison, the OTE indicates a 2.9σ detection.